Original Article

Long non-coding RNA growth arrest-specific 5 inhibits liver fibrogenesis in biliary atresia by interacting with microRNA-222 and repressing IGF1/AKT signaling

Ruoyi Wang, Ya Gao

Department of Pediatric Surgery, The Second Affiliated Hospital of Xi'an Jiaotong University School of Medicine, Xi'an, China

Contributions: (I) Conception and design: Y Gao; (II) Administrative support: Y Gao; (III) Provision of study materials or patients: R Wang; (IV) Collection and assembly of data: R Wang; (V) Data analysis and interpretation: R Wang; (VI) Manuscript writing: Both authors; (VII) Final approval of manuscript: Both authors.

Correspondence to: Ya Gao, MD. Department of Pediatric Surgery, The Second Affiliated Hospital of Xi'an Jiaotong University School of Medicine, No. 157 Xiwu Avenue, Xi'an 710004, China. Email: ygao@mail.xjtu.edu.cn.

Background: Long non-coding RNA growth arrest-specific 5 (lncRNA GAS5) has been shown to inhibit liver fibrosis through serving as a competing endogenous RNA for microRNA-222 (miR-222). Progressive liver fibrosis is a typical characteristic of biliary atresia (BA). However, the role of GAS5/miR-222 and its underlying mechanisms remain largely unknown in BA.

Methods: The expression of GAS5 was determined in the liver and primary hepatic stellate cells (HSCs) of BA patients. Then, the effects of GAS5 on the activation and proliferation of HSCs were evaluated. Furthermore, the interaction between GAS5 and miR-222 was investigated by a luciferase gene report assay. Next, the effects of IGF1/AKT signaling were determined to clarify the downstream mechanism of GAS5. Finally, GAS5 administration was performed to explore its role in an experimental BA mouse model.

Results: GAS5 expression was decreased in liver tissues and HSCs of BA patients, and was inversely correlated with liver fibrosis in BA. Up-regulation of GAS5 in LX-2 cells significantly reduced smooth muscle α-actin (α-SMA) and collagen 1a1 (COL1A1) expression, inhibited cell proliferation and clone formation ability, induced S phase increase, and promoted cell apoptosis. Moreover, GAS5 was negatively regulated by miR-222, which promoted HSCs activation and proliferation, and was positively correlated with liver fibrosis in BA. Additionally, the expressions of IGF1, p-PI3K, and p-AKT were decreased when LX-2 cells over-expressed GAS5, whereas knockdown of IGF1 or AKT significantly decreased α-SMA and COL1A1 expression, suppressed cell proliferation, and enhanced cell apoptosis in LX-2 cells. Furthermore, GAS5 administration significantly increased apoptosis and reduced liver fibrosis, α-SMA and COL1A1 expressions in liver tissues of BA mice.

Conclusions: GAS5 inhibited liver fibrosis in BA by interacting with miR-222 and regulating IGF1/AKT signaling, which may be a therapeutic target to alleviate liver fibrosis in BA.

Keywords: Biliary atresia (BA); liver fibrosis; long non-coding RNA growth arrest-specific 5 (lncRNA GAS5); microRNA-222 (miR-222)

Submitted Aug 10, 2023. Accepted for publication Nov 26, 2023. Published online Dec 22, 2023.
doi: 10.21037/tp-23-424
View this article at: https://dx.doi.org/10.21037/tp-23-424

Introduction

Biliary atresia (BA), a liver disease with a multifaceted pathogenesis, if not treated timely, affects a child's health with rapid progression to end-stage cirrhosis (1). BA is the leading cause of neonatal cholestasis and is characterized by periductular inflammation and fibrosis (2,3). Liver fibrosis is characterized by excessive accumulation of extracellular matrix (ECM) proteins. In addition, hepatic stellate cells (HSCs) have been regarded as the key matrix producing cells in the liver, and activation of HSCs is a major driver for liver fibrosis (4). In response to harmful agents and/or inflammatory cytokines, HSCs could be activated, thereby losing their lipid droplets, and migrating to injured sites where they transform into myofibroblast-like cells (5). Therefore, controlling the proliferation and activation of HSCs may be a potent method to alleviate liver fibrosis in BA.

High throughput transcriptome analysis has shown that only less than 2% of human genes have protein-coding capacity, whereas more than 75% genes represent noncoding RNA (ncRNA) (6,7), including small interfering RNAs (siRNAs), natural antisense transcripts, small nucleolar RNAs, P-element-induced wimpy testis (PIWI)-interacting RNAs, microRNAs (miRNAs), and long non-coding RNAs (lncRNAs) (8). MiRNAs are endogenous small RNA molecules of approximately 22 nucleotides in length (9). MiRNAs have been found to regulate about 30% of human gene expression through specifically binding to the 3'-untranslated region (3'-UTR) of their target gene mRNAs, thereby inhibiting translation or promoting mRNA cleavage (10). Through the regulation of cell proliferation, apoptosis, differentiation, and cell cycle, miRNAs have been shown to be closely implicated in a variety of diseases including BA (11). MiR-222 has been reported to be up-regulated in activated HSCs and its high expression promotes liver fibrotic progression in animal models via targeting protein phosphatase 2A subunit B (PPP2R2A) (12-14). LncRNAs are long ncRNAs (>200 nt) that are also involved in the pathogenesis of BA. In a previous study, Yu *et al.* (15) reported that the expressions of lncRNA growth arrest-specific 5 (GAS5) in fibrotic liver tissues and activated HSCs were low, and that up-regulation of GAS5 repressed activation of primary HSCs *in vitro* and alleviated collagen accumulation *in vivo* via serving as a competing endogenous RNA (ceRNA) for miR-222. These findings suggested a key role of GAS5/miR-222 in liver fibrosis. However, the role of GAS5/miR-222 and its underlying mechanisms still remain largely undefined in BA.

Activation of HSCs is regulated by many signal transduction pathways, including the PI3K/AKT pathway (16). Once PI3K is activated, it will phosphorylate its downstream effector, AKT, thereby accelerating cell growth and survival. IGF1, which is mainly synthesized by the liver, has been thought to be an important activator of PI3K/AKT signaling (17). IGF1 and IGF2 are functionally similar to insulin but have much higher growth-promoting effects on many cell types, including hepatocytes (18), and are thought to play a crucial role in the pathogenesis of chronic liver disease (19).

In the present study, we explored of the role of GAS5/miR-222 in the liver fibrogenesis of BA, and further elucidated that IGF1/AKT signaling was the downstream mechanism of GAS5 through both *in vivo* and *in vitro* experiments. We present this article in accordance with the MDAR reporting checklist (available at https://tp.amegroups.com/article/view/10.21037/tp-23-424/rc).

Highlight box

Key findings

- Growth arrest-specific 5 (GAS5) inhibited liver fibrosis in biliary atresia (BA) by interacting with microRNA-222 (miR-222) and regulating IGF1/AKT signaling.

What is known and what is new?

- Progressive liver fibrosis is the main cause of end-stage liver disease in BA. Long non-coding RNA GAS5 has been demonstrated to alleviate liver fibrogenesis through functioning as a competing endogenous RNA for miR-222. However, the role of GAS5 and its underlying mechanisms remain elusive in BA.
- This study firstly explored the role of GAS5/miR-222 and its underlying mechanism in the liver fibrogenesis of BA.

What is the implication, and what should change now?

- GAS5 played a beneficial role in BA through inhibiting activation and proliferation of hepatic stellate cells (HSCs) by interacting with miR-222 and repressing IGF1/AKT signaling, which indicated that GAS5 was a therapeutic target to alleviate liver fibrosis in BA.

Methods

Tissue samples

A total of 24 BA patients and 24 healthy control subjects (normal liver tissue adjacent to the excised hepatoblastoma) were randomly recruited from Department of Pediatric Surgery, The Second Affiliated Hospital of Xi'an Jiaotong University School of Medicine. Intraoperative

Table 1 Clinical information for all patients

Group	Control (n=24)	BA (n=24)
Age (month) (mean ± SD)	20.1±10.6****	2.4±0.6
Gender, n		
Male/female	13/11^{ns}	10/14
Laboratory examination (mean ± SD)		
ALT (U/L)	20.2±8.1****	152.8±100.2
AST (U/L)	44.0±21.6****	254.4±163.8
ALB (g/L)	39.1±8.2^{ns}	38.5±4.2
TBIL (μmol/L)	10.6±11.2****	170.2±38.6
DBIL (μmol/L)	2.2±1.5****	128.2±24.5
ALP (U/L)	200.2±102.6****	676.8±220.5
GGT (U/L)	28.2±20.8****	590.8±466.3
TBA (μmol/L)	9.5±6.2****	112.8±36.3
Grades of inflammation, n (%)		
G1	–	1 (4.2)
G2	–	8 (33.3)
G3	–	15 (62.5)
Stages of fibrosis, n (%)		
S0	–	0
S1	–	0
S2	–	9 (37.5)
S3	–	9 (37.5)
S4	–	6 (25.0)

****, P<0.0001; ns, not significant. BA, biliary atresia; SD, standard deviation; ALT, alanine aminotransferase; AST, aspartate aminotransferase; ALB, albumin; TBIL, total bilirubin; DBIL, direct bilirubin; ALP, alkaline phosphatase; GGT, gamma-glutamyl transpeptidase; TBA, total bile acid.

cholangiography was used for BA diagnosis, and hepatic histopathology was applied for the hepatoblastoma diagnosis. Their clinical information is presented in *Table 1*. Liver tissues were obtained from patients undergoing partial liver resection or liver biopsy. This study was conducted in accordance with the Declaration of Helsinki (as revised in 2013). This study was approved by the Ethics Committee of the Second Affiliated Hospital of Xi'an Jiaotong University School of Medicine (No. 2018-2147), and written informed consent was obtained from the parents or legal guardians of the children prior to the start of the study.

Cell culture

The isolation of primary HSCs was performed as described previously (20). In summary, human liver tissues were perfused with EGTA (Sigma, St. Louis, MO, USA, 67-42-5), Pronase (Sigma, PRON-RO), and collagenase NB 4G (Nordmark, Uetersen, Germany, S1746501) for 30 min *in situ* at 37 ℃. After centrifugation at 25 g for 5 min and 400 g for 10 min, HSCs were separated from the non-parenchymal cells by density gradient centrifugation. HSCs were maintained in DMEM (Gibco, Waltham, MA, USA) containing 10% fetal bovine serum (FBS) (Gibco) and 1% penicillin/streptomycin in a humidity incubator at 37 ℃ with 5% CO_2.

Human immortalized HSC line LX-2 was purchased from Sigma (SCC064) and cultured in DMEM, supplemented with 2 mM L-glutamine, 1% penicillin/streptomycin (Thermo, Waltham, MA, USA, 15070063) and 10% FBS (Thermo, 15070063).

Transfection of cells

SiRNAs targeting the human AKT (gene symbol AKT1, No. SR300143) and IGF1 (No. SR302343), or negative control (NC) were purchased from OriGene (Wuxi, China) and used to transfect LX-2 cells to down-regulate AKT and IGF1 expression, respectively. For transfection studies, lipofectamine 2000 transfected reagent (Invitrogen, Carlsbad, CA, USA, 11668500) was used. Inhibitor-miR-222 and the overexpressing lentivirus vector of GAS5 (Vector-GAS5), were synthesized by GenePharma (Shanghai, China), and used to knockdown miR-222 and up-regulate GAS5, respectively.

Real-time quantitative polymerase chain reaction (qPCR)

Total RNA was exacted from liver tissues and HSCs using a GenElute™ Total RNA Purification Kit (Sigma, RTN70). After quantification of RNA by NanoDrop (Thermo, 701-058112), a total of 1 μg RNA was reverse transcribed into complementary DNA (cDNA) for qPCR analysis. MRNA qPCR kits used in this study were purchased from Takara (Beijing, China, RR047A, RR820A). For miRNA quantification, stem-loop RT primers were used to reverse miRNAs according to the miRNA 1st strand cDNA synthesis kit (Vazyme, Nanjing, China, MR101-01). Subsequently, qPCR was performed using miRNA Universal SYBR qPCR Master Mix (Vazyme, MQ101-01)

Table 2 Primer sequences for real-time quantitative polymerase chain reaction analysis in humans

Gene	Primer sequences (5'-3')
α-SMA	F: CTATCCCCGGGACTAAGACG
	R: GGGCAACACGAAGCTCATTG
COL1A1	F: AGTGGTTTGGATGGTGCCAA
	R: GCACCATCATTTCCACGAGC
GAS5	F: ACTCAAGCCATTGGCACACA
	R: TCCACACAGTGTAGTCAAGCC
IGF1	F: GCTCTTCAGTTCGTGTGTGGA
	R: GCCTCCTTAGATCACAGCTCC
AKT1	F: AGCGACGTGGCTATTGTGAAG
	R: GCCATCATTCTTGAGGAGGAAGT
GAPDH	F: CCAGCTACTCGCGGCTTTAC
	R: GTTCACACCGACCTTCACCA
miR-222	RT: GTCGTATCCAGTGCAGGGTCCGAGGTATT CGCACTGGATACGACAGGATC
	F: GACTCAGTAGCC AGTGTA
	R: GTGCAGGGTCCGAGGT
U6	RT: AACGCTTCACGAATTTGCGT
	F: CTCGCTTCGGCAGCACA
	R: AACGCTTCACGAATTTGCGT

Table 3 Primer sequences for real-time quantitative polymerase chain reaction analysis in mouse

Gene	Primer sequences (5'-3')
GAS5	F: GGAAGCTGGATAACAGAGCGA
	R: GGTATTCCTTGTAATGGGACCAC
GAPDH	F: CATCACTGCCACCCAGAAGACTG
	R: ATGCCAGTGAGCTTCCCGTTCAG
miR-222	RT: GTCGTATCCAGTGCAGGGTCCGAGGTATT CGCACTGGATACGACAGACCC
	F: CGCGAGCTACATCTGGCTACT
	R: AGTGCAGGGTCCGAGGTATT
U6	RT: AACGCTTCACGAATTTGCGTG
	F: GCTCGCTTCGGCAGCACA
	R: GAGGTATTCGCACCAGAGGA

with specific forward primers and universal reverse primers. GAPDH and U6 were used as internal controls. Relative gene expression was calculated by the $2^{-\Delta\Delta Ct}$ method. Primer sequences used in this study are listed in *Tables 2,3*.

Western blot analysis

Proteins from cells and tissues were extracted using RIPA lysis buffer (Thermo, 89900) containing protease and phosphatase inhibitors (Thermo, 78440). After centrifugation at 4 ℃ for 30 min, protein samples were quantified by a bicinchoninic acid (BCA) method (Beyotime, Shanghai, China, P0009). Subsequently, protein samples were loaded onto a 10% SDS-polyacrylamide gel and separated by electrophoresis, and transferred to PVDF membranes (Merck Millipore, Darmstadt, Germany, ISEQ00010). Membranes were blocked with 5% non-fat milk dissolved in TBST, and incubated overnight at 4 ℃ with primary antibodies directed against the following proteins: IGF1 (Abcam, Cambridge, UK, ab9572, 1:2,000), AKT (CST, Boston, MA, USA, 9272, 1:1,000), p-AKT (CST 9275, 1:1,000), PI3K (CST 4292, 1:1,000), p-PI3K (Abcam ab138364, 1:1,000) or GAPDH (CST 2118, 1:1,000). Membranes were washed three times with TBST and incubated with HRP-conjugated anti-rabbit secondary antibody (Abcam ab150077, 1:5,000) for 1 h at room temperature. After washing three times with TBST, protein bands were visualized by an ECL regent (Thermo, 32209) and quantification analysis was carried out by ImageJ software.

Methyl thiazolyl tetrazolium (MTT) assay

To assess the effect of lncRNA-GAS5/miR-222 on cell proliferation, a MTT assay was performed. In brief, HSCs at a density of 5×10^3 cells/well were seeded into 96-well plates and cultured in RPMI-1640 medium with 10% FBS. At 1, 2, 3, 4, 5, and 6 days after seeding, 20 μL of sterile MTT dye (5 mg/mL, Sigma, 298-93-1) was added to each well and cells were incubated for 4 h. Then, cells were treated with 200 μL of DMSO for 30 min, and spectrometric absorbance at 570 nm wavelength was measured using a microplate reader (BioTek, Winooski, VT, USA).

Clone formation assay

A total of 3×10^3 LX-2 cells diluted in 100 μL complete

culture medium were placed into 6-well plates at 37 ℃ and 5% CO_2 for 12 h. Subsequently, cells were treated with Vector-GAS5 or inhibitor-miR-222 and incubated at 37 ℃ with 5% CO_2. The medium was replaced every 2 days until 14th day post-treatment. Next, cells were washed with PBS twice, fixed with 5% paraformaldehyde for 30 min, and stained with 0.1% crystal violet solution (Sigma, 548-62-9) for 30 min. Cell clone formation ability was evaluated by counting visible colonies.

Flow cytometry

Cell apoptosis was assessed by flow cytometry using an Annexin V-FITC/PI kit (Thermo, 331200) in accordance with the manufactory's guidelines. Briefly, cells were collected and washed once with PBS 48 h post-treatment. Then, each sample was incubated with Annexin V-FITC and PI solution and incubated for 15 min in the dark at room temperature. Fluorescent signals reflecting cell apoptosis were evaluated by flow cytometry within 1 h. Cells in the $FITC^-/PI^-$ quadrant represented live cells, $FITC^+/PI^-$ represented early apoptotic cells, and $FITC^+/PI^+$ represented late apoptotic cells.

For cell cycle detection, cells were seeded in triplicate in 12-well plates and incubated in FBS-free culture medium for 24 h prior to different treatments. At 48 h after treatments, cells including both the floating and attached cells were harvested and fixed with 70% ethanol for 3 h at 4 ℃, followed by incubation with 20 μg/mL of RNase (Thermo, EN0531) for 30 min at 37 ℃. Then, cells were stained with PI solution (5 μg/mL) for 30 min at 4 ℃ in the dark, and cell cycle phases were analyzed by flow cytometry FlowJo software.

Luciferase gene report assay

Cells were transiently co-transfected with the luciferase reporter plasmid encoding GAS5 wide type (wide-GAS5) or mutated type (mut-GAS5, the binding sites between GAS5 and miR-222 were mutated) (GenePharma), and mimic-miR-222 or mimic-NC. Luciferase activities were measured 48 h after transfection using the Dual-Luciferase Reporter Assay System (Promega, Madison, WI, USA, E1910). Renilla luciferase activity of the firefly was used as a normalized control.

In vivo studies

Pregnant Balb/c mice at 10–12 weeks of age were purchased from SLAC Inc (Shanghai, China). Animals were kept in a specific pathogen-free facility under 12 h-light/12 h-dark conditions with free access to food and water. After 1 week of acclimatization, experimental BA models were established in newborn mice within 24 h after birth (21). Briefly, mice were injected with 20 μL of 1.2×10^5 FFU/mL of RRV MMU 18006 purchased from ATCC (Rockefeller, MD, USA, VR-1739). An equivalent amount of 0.9% NaCl solution was used as a control. Infected mice that died within the first 2 days or that were not fed by their mothers were excluded. Then, BA mice were given 200 μL Vector-GAS5 (5×10^9 TU/mL) through intraperitoneal injection. At 14 days after Vector-GAS5 administration, liver samples were collected for Masson and immunohistochemistry analyses. A total of 8 mice were included in each group (control, BA, BA + GAS5) for the subsequent analysis. Experiments were performed in the Laboratory Animal Center of Xi'an Jiaotong University under a project license [No. SYXK (Shaanxi) 2020-005] granted by the Science and Technology Department of Shaanxi Province. All animal operations were performed in accordance with institutional and national guidelines and regulations for the care and use of laboratory animals.

Terminal deoxynucleotidyl transferase-mediated dUTP nick end labeling (TUNEL) staining

Mice liver tissues were cut into 4-μm slides, then sections were fixed in 4% paraformaldehyde at room temperature for 1 h and treated with 0.1% Triton X-100 on ice for 2 min. Next, sections were washed three times with PBS and incubated in FITC-marked 50 μL TUNEL (Abcam, ab66108) at 37 ℃ for 1 h. Finally, TUNEL staining was observed using a fluorescence microscope (Leica DM IL LED).

Immunohistochemistry staining

For immunohistochemistry analysis, 4-μm sections were deparaffinized, rehydrated, and blocked with 5% goat serum for 2 h at room temperature. Then, sections were incubated with an antibody against collagen 1a1 (COL1A1; Abcam, ab34710, 1:200) or smooth muscle α-actin (α-SMA, Abcam, ab5694, 1:200) overnight at 4 ℃.

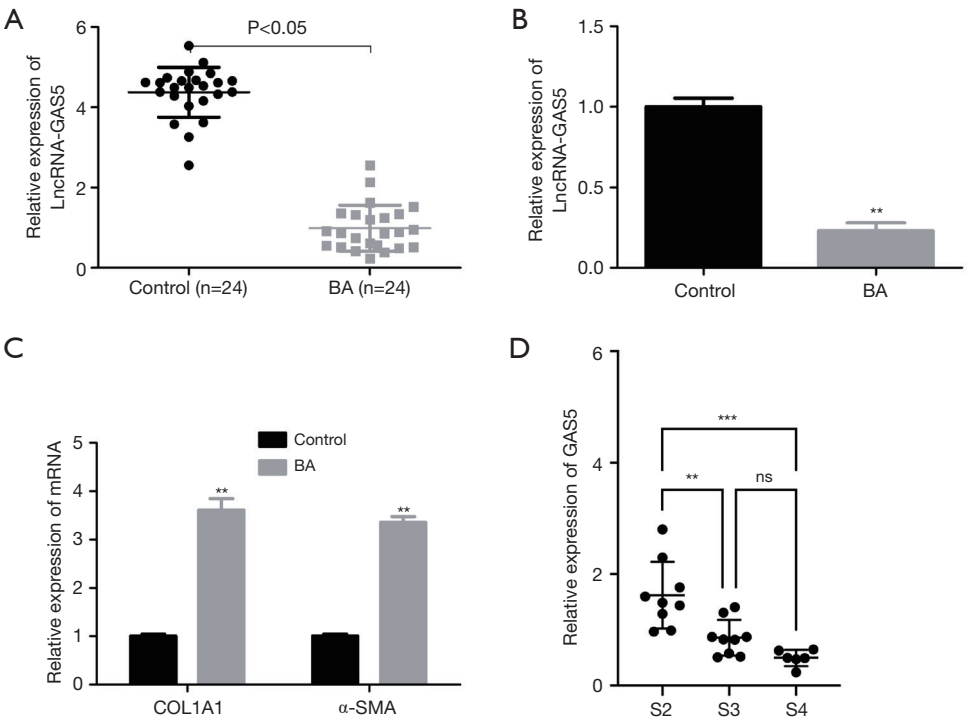

Figure 1 GAS5 is down-regulated in BA patients. (A) GAS5 expression in liver tissues from control individuals or BA patients were determined by qPCR. (B) GAS5 expression in HSCs from control individuals or BA patients was determined by qPCR. (C) qPCR analysis of mRNA expression levels of α-SMA and COL1A1 in HSCs from control individuals or BA patients. (D) GAS5 expression in BA patients with different stages of fibrosis. **, P<0.01; ***, P<0.001. BA, biliary atresia; qPCR, quantitative polymerase chain reaction; α-SMA, smooth muscle α-actin; COL1A1, collagen 1a1; HSC, hepatic stellate cell.

Sections were washed three times with PBS, followed by incubation with horseradish peroxidase-labeled secondary antibody for 30 min at room temperature. Finally, the staining was visualized by staining with DAB (GeneTech, Shanghai, China, GK500710).

Statistical analysis

Data were presented as the mean ± standard deviation. Statistical analysis was performed by Student's *t*-test or one way ANOVA test with P<0.05 as the significance level using GraphPad Prism 9 software. Each experiment was independently performed at least three times.

Results

LncRNA-GAS5 is down-regulated in patients with BA

To explore the function of GAS5/miR-222 in the pathogenesis of BA, we first determined the expression of GAS5 in liver tissues and HSCs from control individuals and BA patients. When compared with the control group, GAS5 expression was down-regulated in liver tissues of BA patients (*Figure 1A*), and HSCs isolated from BA patients (*Figure 1B*). We also evaluated the expressions of α-SMA and COL1A1 in HSCs from control individuals and BA patients. Our results showed that mRNA levels of COL1A1 and α-SMA were elevated in the BA group when compared with the control group (*Figure 1C*). Furthermore, the expressions of GAS5 were declined with the elevated stages of fibrosis in BA (*Figure 1D*). These findings indicated that down-regulation of GAS5 was associated with BA liver fibrogenesis.

Overexpression of GAS5 represses the activation and proliferation of HSCs

Next, we investigated the role of GAS5 in the activation and proliferation of HSCs by carrying out a gain-of-function assay. Our data showed that Vector-GAS5 transfection

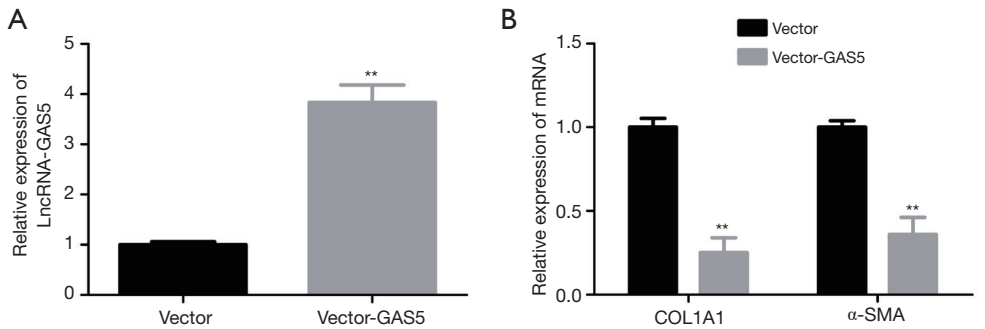

Figure 2 Up-regulation of GAS5 represses activation of hepatic stellate cells. (A) At 48 h after transduction of LX-2 cells with Vector-GAS5 or Vector, the expression of GAS5 was determined by qPCR. (B) The effects of GAS5 up-regulation on the expression of α-SMA and COL1A1 were evaluated by qPCR. **, P<0.01. qPCR, quantitative polymerase chain reaction; α-SMA, smooth muscle α-actin; COL1A1, collagen 1a1.

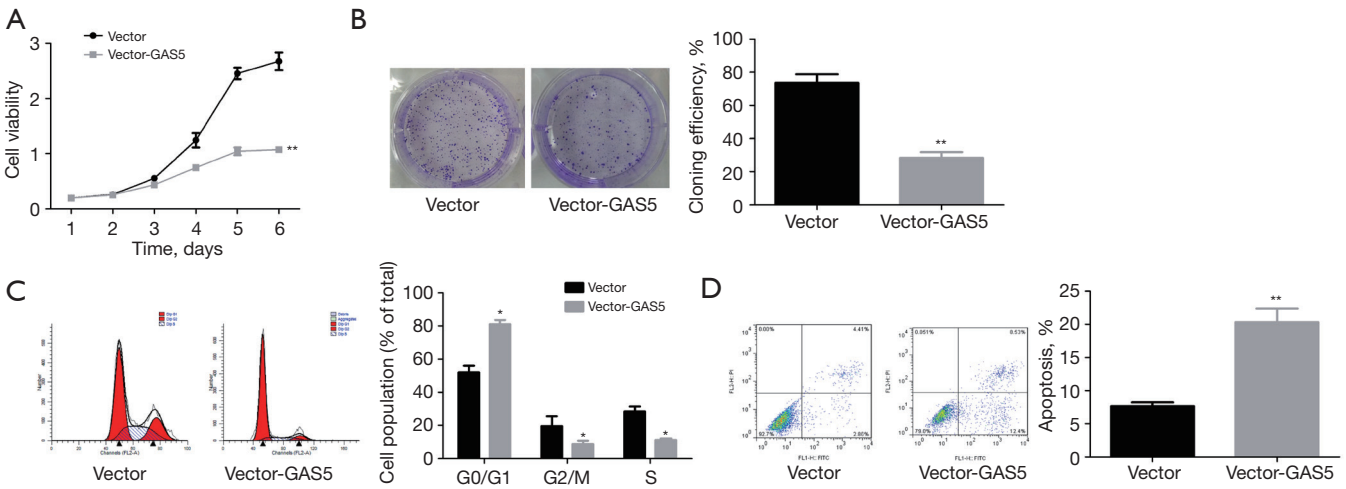

Figure 3 Up-regulation of GAS5 represses the proliferation of LX-2 cells. (A) At indicated time points, an MTT assay was used to determine the cell viability after LX-2 cells were infected with Vector or Vector-GAS5. (B) Cell clone formation ability was tested by clone formation assay after LX-2 cells were infected with Vector or Vector-GAS5 (crystal violet staining). (C) Effect of GAS5 on cell cycle phase was determined by flow cytometry using PI staining. (D) Cell apoptosis was determined by flow cytometry using Annexin V/PI double staining. *, P<0.05; **, P<0.01. MTT, methyl thiazolyl tetrazolium; PI, propidium iodide.

significantly enhanced GAS5 expression in LX-2 cells (*Figure 2A*). When compared with the vector group, GAS5 up-regulation significantly reduced the expression of α-SMA and COL1A1 (*Figure 2B*), inhibited cell proliferation, and clone formation ability (*Figure 3A,3B*), induced G0/G1 phase arrest and reductions in G2/M and S phases (*Figure 3C*), and increased cell apoptosis (*Figure 3D*). Together, these discoveries revealed that GAS5 up-regulation inhibited proliferation and activation of HSCs.

GAS5 interacts with miR-222

Next, we explored the crosstalk between GAS5 and miR-222 in HSCs. When compared with the control group, miR-222 was up-regulated in the liver tissues (*Figure 4A*) and HSCs (*Figure 4B*) of BA patients. In contrast to GAS5, miR-222

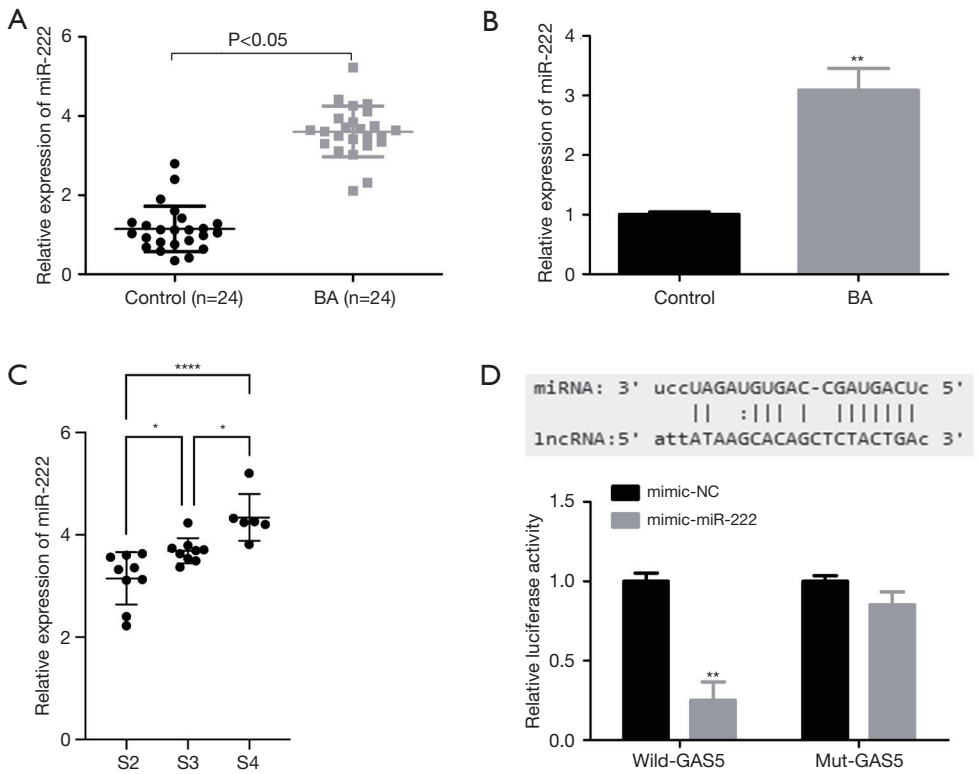

Figure 4 GAS5 interacts with miR-222. (A,B) miR-222 levels in liver tissues and hepatic stellate cells from healthy individuals and BA patients were determined by qPCR analysis. (C) miR-222 levels in BA patients with different stages of fibrosis. (D) A luciferase gene report assay was performed to evaluate the effects of miR-222 on the expression of GAS5. *, P<0.05; **, P<0.01; ****, P<0.0001. BA, biliary atresia; qPCR, quantitative polymerase chain reaction; NC, negative control.

demonstrated higher expressions with the increased stages of fibrosis in BA (*Figure 4C*). Results from bioinformatics analysis showed that GAS5 bound to the 3'UTR of miR-222 (*Figure 4D*). Moreover, up-regulation of miR-222 decreased the expression of GAS5 in LX-2 cells (*Figure 4D*). Together, these findings demonstrated that GAS5 interacted with miR-222, and that miR-222 might exert an opposite role in BA liver fibrogenesis from GAS5.

Down-regulation of miR-222 represses the activation and proliferation of HSCs

Subsequently, we investigated the function of miR-222 in activation and proliferation of HSCs. *Figure 5A* shows the knockdown efficiency of inhibitor-miR-222 in LX-2 cells. When compared with the inhibitor-NC group, miR-222 down-regulation significantly reduced the expression of α-SMA and COL1A1 (*Figure 5B*), inhibited cell proliferation and clone formation ability (*Figure 5C,5D*), induced a G0/G1 phase arrest and reductions in S phase (*Figure 5E*), and increased cell apoptosis (*Figure 5F*). Altogether, these results indicated that down-regulation of miR-222 repressed activation and proliferation of HSCs.

GAS5 up-regulation represses the activation and proliferation of HSCs through inhibiting IGF1/AKT signaling

The expressions of IGF1 and AKT (gene symbol *AKT1*) were elevated in the liver tissues and HSCs of BA when compared with controls (*Figure 6A,6B*). As expected, IGF1 and AKT were also up-regulated with the increased stages of fibrosis in BA (*Figure 6C*). We next explored whether IGF1/AKT signaling was involved in the suppression of HSCs activation and proliferation mediated by GAS5-up-regulation. When compared with the vector group,

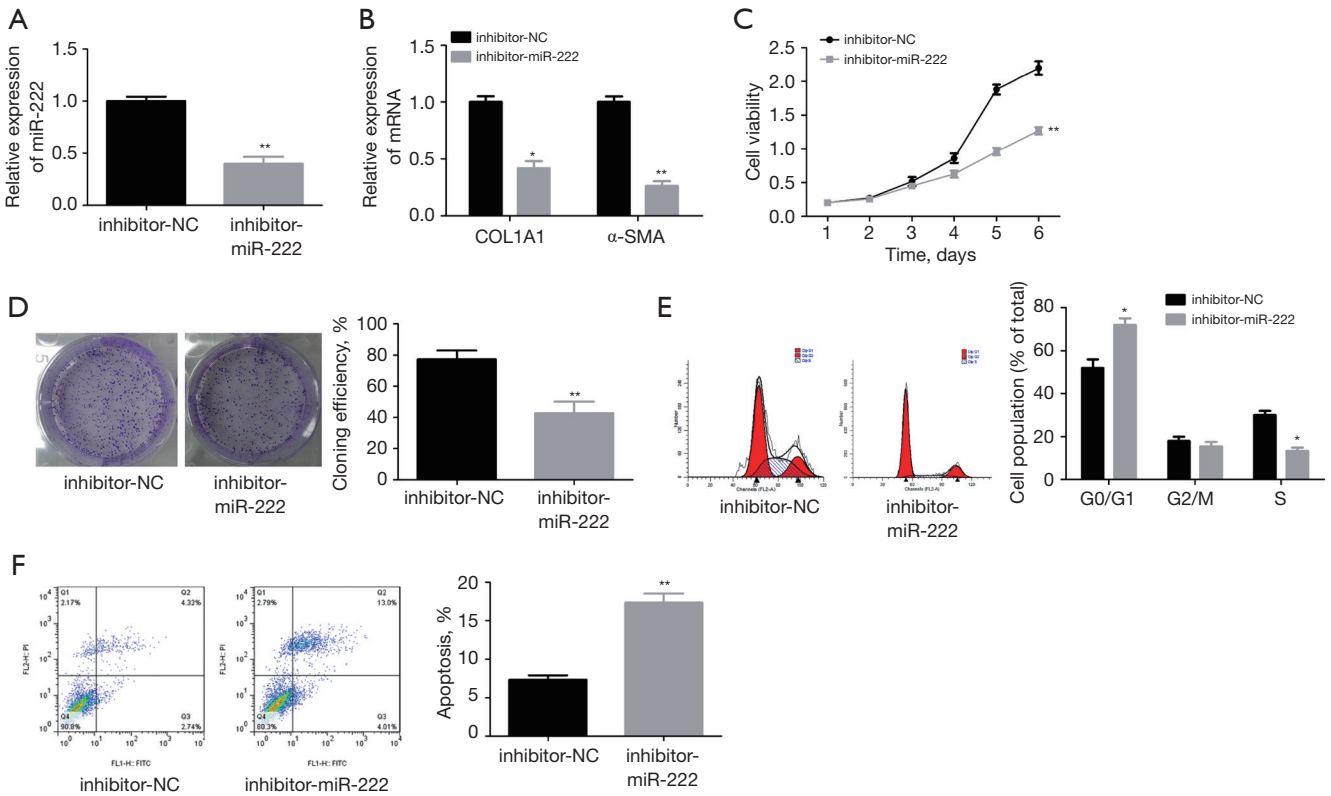

Figure 5 Down-regulation of miR-222 represses activation and proliferation of hepatic stellate cells. (A) The knockdown efficiency of inhibitor-miR-222 was evaluated by qPCR. (B) qPCR was performed to determine mRNA levels of α-SMA and COL1A1 after LX-2 cells were transfected with inhibitor-NC or inhibitor-miR-222. (C) MTT analysis of cell viability. (D) Cell clone formation ability was evaluated by clone formation assay after LX-2 cells were transfected with inhibitor-NC or inhibitor-miR-222 (crystal violet staining). (E) The effect of miR-222 on the cell cycle was determined by flow cytometry using PI staining. (F) Cell apoptosis was determined by flow cytometry using Annexin V/PI double staining. *, P<0.05; **, P<0.01. α-SMA, smooth muscle α-actin; COL1A1, collagen 1a1; qPCR, quantitative polymerase chain reaction; MTT, methyl thiazolyl tetrazolium; NC, negative control; PI, propidium iodide.

the expression levels of IGF1, p-PI3K, and p-AKT were reduced when LX-2 cells were transfected with Vector-GAS5 (*Figure 6D*). Subsequently, we explored the effects of IGF1 and AKT on the activation and proliferation of HSCs through a loss-of-function assay. When compared with the control group, siRNAs-1 targeting human *AKT* and *IGF1* genes significantly decreased the expression of AKT and IGF1 at both the mRNA and protein levels (*Figure 6E,6F*). In addition, cell proliferation was inhibited (*Figure 6G*) whereas cell apoptosis was increased (*Figure 6H*) when LX-2 cells were down-regulated for AKT or IGF1, and the expression of α-SMA and COL1A1 was decreased (*Figure 6I*). Thus, these results demonstrated that inactivation of IGF1/AKT signaling was strongly implicated in the inhibition activation and proliferation of HSCs induced by GAS5 up-regulation.

GAS5 alleviates the progression of BA in vivo

Finally, we investigated the function of GAS5 in BA progression through establishing experimental BA mice models. Consistent with the results in humans, GAS5 was down-regulated, whereas miR-222 was up-regulated in BA mice when compared with controls (*Figure 7A*). Furthermore, BA mice with higher stage of fibrosis also demonstrated lower GAS5 and higher miR-222 levels (*Figure 7B*). When compared with the BA group, cell apoptosis was enhanced (*Figure 7C*), and liver fibrosis and

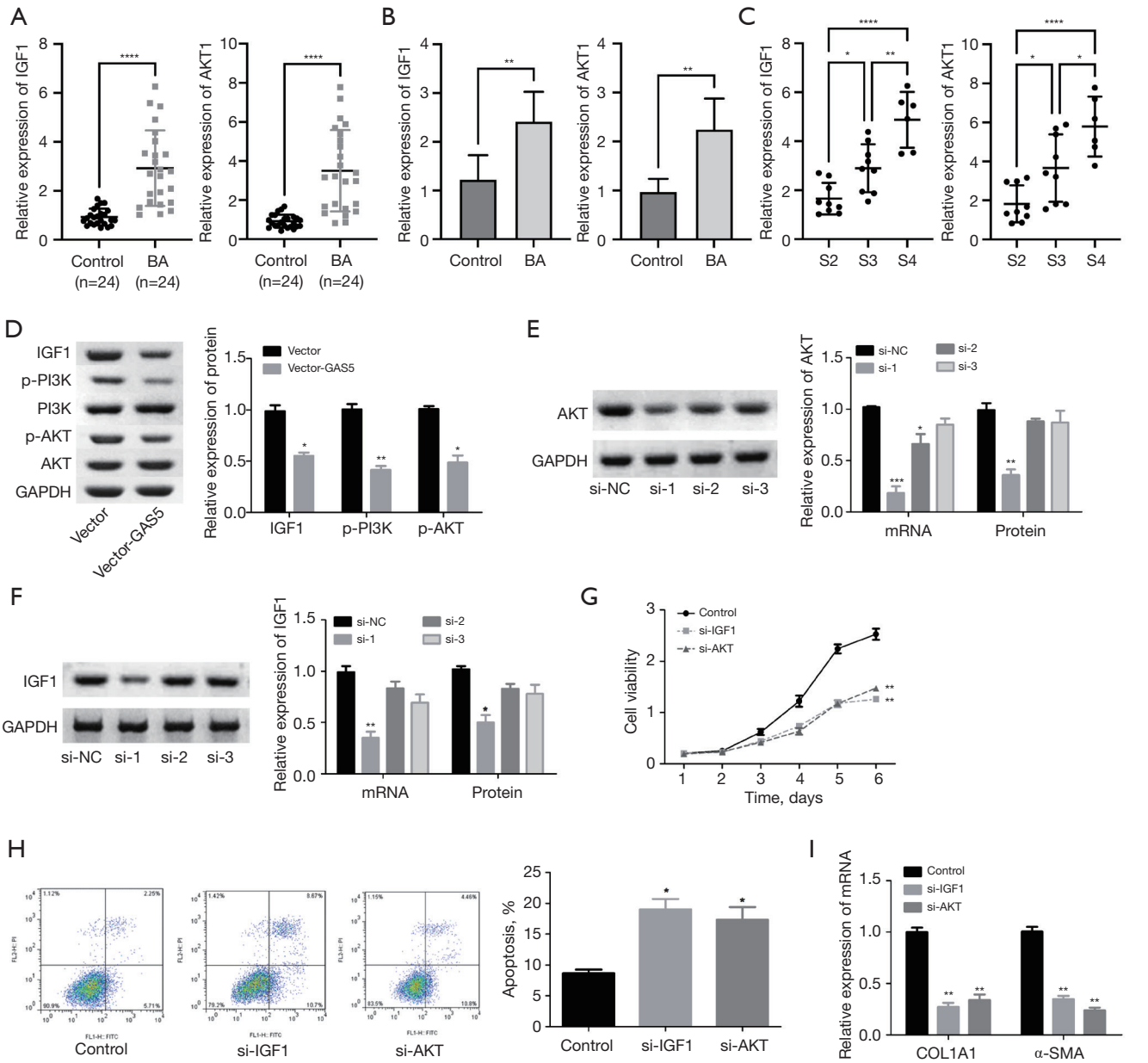

Figure 6 The IGF1/AKT signaling pathway is involved in GAS5-induced biliary atresia alleviation. (A,B) The mRNA levels of IGF1 and AKT (gene symbol AKT1) in liver tissues and hepatic stellate cells from control individuals or BA patients were determined by qPCR. (C) The expressions of IGF1 and AKT in BA patients with different stages of fibrosis. (D) The expressions of IGF1, p-PI3K, PI3K, p-AKT, and AKT were evaluated by western blot analysis after LX-2 cells were infected with Vector or Vector-GAS5. (E,F) Western blot analysis of knockdown efficiencies of si-AKT and si-IGF1 in LX-2 cells. (G) The viability of LX-2 cells in control, si-AKT, and si-IGF1 groups was determined by MTT assay. (H) Cell apoptosis was determined by flow cytometry. (I) The role of AKT or IGF1 knockdown in α-SMA and COL1A1 expressions was measured by qPCR. *, P<0.05; **, P<0.01; ***, P<0.001; ****, P<0.0001. qPCR, quantitative polymerase chain reaction; BA, biliary atresia; MTT, methyl thiazolyl tetrazolium; NC, negative control; α-SMA, smooth muscle α-actin; COL1A1, collagen 1a1.

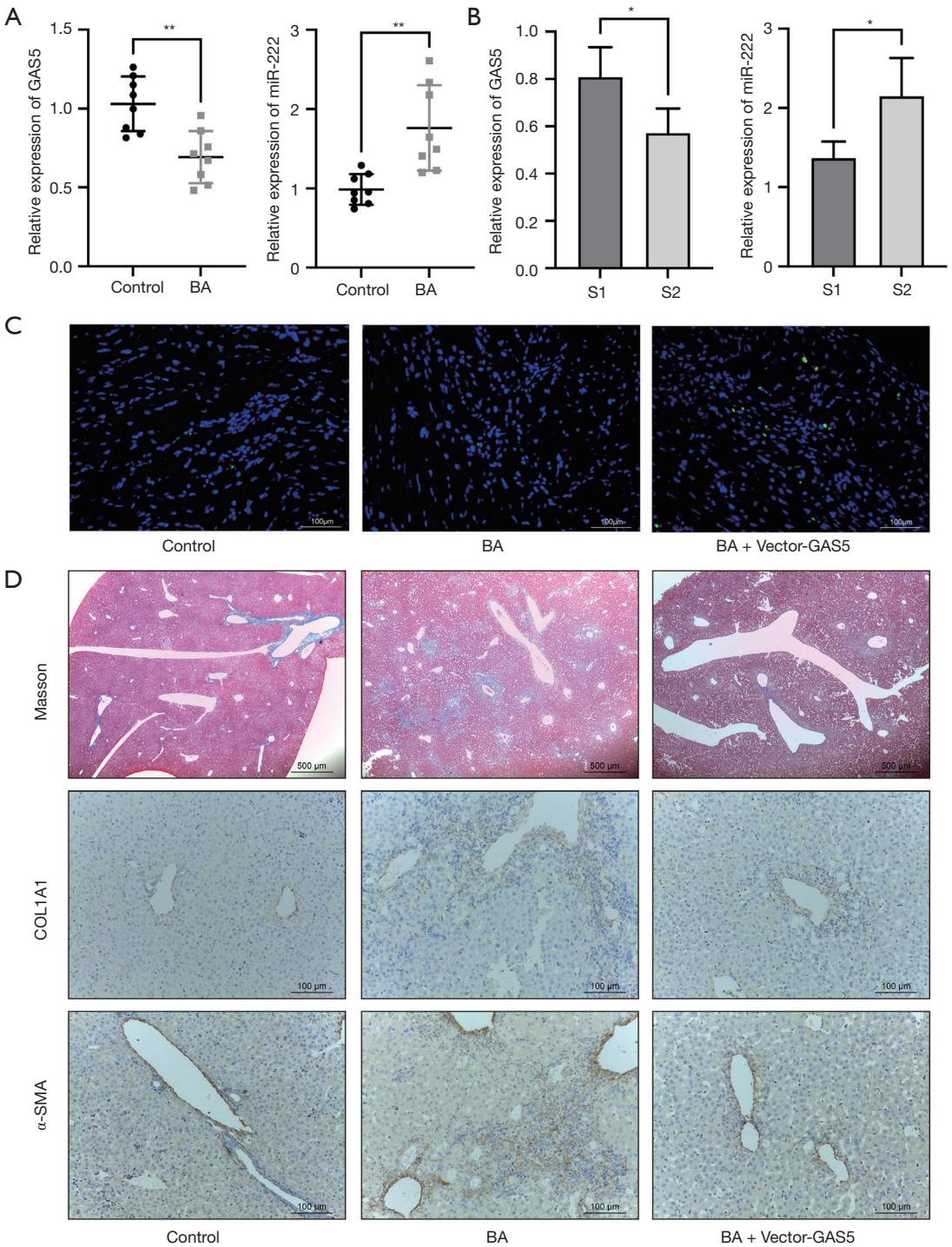

Figure 7 GAS5 administration alleviated liver fibrosis in experimental BA. (A) The expressions of GAS5 and miR-222 in experimental BA and controls. (B) The expressions of GAS5 and miR-222 in BA mice with different stages of fibrosis. (C) TUNEL assay was used to evaluate cell apoptosis in the BA liver tissue (200× magnification). (D) Masson (40×) and IHC staining (200×) were used to evaluate the stages of fibrosis and the expressions of α-SMA and COL1A1 in the BA liver tissue. *, P<0.05; **, P<0.01. BA, biliary atresia; TUNEL, Terminal deoxynucleotidyl transferase-mediated dUTP nick end labeling; IHC, immunohistochemistry.

the expressions of COL1A1 and α-SMA were reduced (*Figure 7D*) in liver tissues from BA mice that overexpressed GAS5.

Discussion

BA is a devastating disease, which affects newborns within a few months after birth, and is characterized by liver inflammation, fibrosis, and bile duct obstruction (22). Previous studies have shown that the incidence of BA was higher in Southeast Asia, such as China and Japan (1/9,600–1/5,300) versus North America and Western Europe (1/16,000) (23-25). Although the pathogenesis of BA is unclear, the fibrotic obstruction of extrahepatic bile ducts is reasonable and acceptable (1). Importantly, hyper-activation of HSCs plays a crucial role in the progression of liver fibrosis through facilitating the synthesis and accumulation of collagen and ECM (26). When focusing on the activation and proliferation of HSCs, we found that when compared to control subjects, GAS5 was down-regulated in the liver tissue and HSCs derived from BA patients. Moreover, it has been shown that GAS5 up-regulation in LX-2 cells, the common immortalized human HSCs with a myofibroblast-like phenotype (27), significantly repressed the expression of α-SMA and COL1A1, indicators of HSC activation (28), reduced cell viability and promoted apoptosis, thereby suggesting that GAS5 played a protective role against liver fibrosis progression through regulating the activation of HSCs.

GAS5 was initially derived from mouse NIH3T3 cells through subtraction hybridization (29), and has previously been strongly implicated in the progression of some types of cancers, including breast cancer, prostate cancer, and gastric cancer (30-32). Consistently, Yu *et al.* (15) revealed that GAS5 was involved in the progression of liver fibrogenesis. In detail, the expression of GAS5 was decreased in fibrotic liver tissues of mice, rats, and humans, and activated HSCs, and GAS5 up-regulation significantly inhibited primary HSCs activation and reduced collagen accumulation in fibrotic liver tissues by direct binding to miR-222, one of the most studied miRNAs. MiR-222 has been shown to exacerbate the progression of BA through accelerating the progression of liver fibrosis (12,14). In the present study, we further explored the interaction between miR-222 and GAS5 and their roles in BA progression. A luciferase gene report assay showed that GAS5 was a direct target of miR-222, and that miR-222 up-regulation using mimic transfection decreased GAS5 expression, which was consistent with the findings presented in previous studies (15). On the contrary, miR-222 was highly expressed in HSCs and the liver tissue of BA patients, and knockdown of miR-222 significantly repressed activation and proliferation and promoted apoptosis of LX-2 cells, thereby confirming that high expression of miR-222 aggravated liver fibrosis, which then promoted the progression of BA.

Mechanically, we found that GAS5 up-regulation repressed activation of the IGF1/AKT pathway. Noticeably, knockdown of either IGF1 or AKT repressed the expression of α-SMA and COL1A1, reduced cell proliferation, and enhanced cell apoptosis, suggesting that GAS5 up-regulation prevented the progression of liver fibrosis in BA through repressing IGF1/AKT signaling. Mounting evidence has demonstrated that increased AKT activation could lead to advanced fibrosis (33) and inhibition of the PI3K/AKT signaling pathway was found in many processes of liver fibrosis mitigation. For example, a reduction in p-AKT expression was closely associated with miR-145 or adiponectin-induced inhibition of liver fibrosis and HSC activation (34,35).

Although the etiology of BA remains largely unclear, data have confirmed that a perinatal viral infection may be a possible pathogenic mechanism involved (36). In the experimental murine model of BA, RRV infection of newborn Balb/c mice resulted in a pathological phenotype that was similar to human BA (37,38). Therefore, we established BA models via RRV administration to explore the anti-fibrotic role of GAS5 in BA mice. Our results showed that administration of GAS5-overexpressing lentivirus (Vector-GAS5) significantly enhanced apoptosis and reduced liver fibrosis and α-SMA and COL1A1 expressions in the liver tissue from experimental BA mice.

Conclusions

In conclusion, in the present study, we clarify that GAS5 plays a beneficial role in BA through inhibiting activation and proliferation of HSCs by interacting with miR-222 and repressing IGF1/AKT signaling. Our study is the first to elucidate the role of GAS5 in BA, and provides evidence on the possibility of GAS5 as a therapeutic target to alleviate liver fibrosis in BA.

Acknowledgments

Funding: This study received financial support from the Natural Science Foundation of China (No. 82170531).

Footnote

Reporting Checklist: The authors have completed the MDAR reporting checklist. Available at https://tp.amegroups.com/article/view/10.21037/tp-23-424/rc

Data Sharing Statement: Available at https://tp.amegroups.com/article/view/10.21037/tp-23-424/dss

Peer Review File: Available at https://tp.amegroups.com/article/view/10.21037/tp-23-424/prf

Conflicts of Interest: Both authors have completed the ICMJE uniform disclosure form (available at https://tp.amegroups.com/article/view/10.21037/tp-23-424/coif). The authors have no conflicts of interest to declare.

Ethical Statement: The authors are accountable for all aspects of the work in ensuring that questions related to the accuracy or integrity of any part of the work are appropriately investigated and resolved. This study was conducted in accordance with the Declaration of Helsinki (as revised in 2013). This study was approved by the Ethics Committee of the Second Affiliated Hospital of Xi'an Jiaotong University School of Medicine (No. 2018-2147), and written informed consent was obtained from the parents or legal guardians of the children prior to the start of the study. Experiments were performed in the Laboratory Animal Center of Xi'an Jiaotong University under a project license [No. SYXK (Shaanxi) 2020-005] granted by the Science and Technology Department of Shaanxi Province. All animal operations were performed in accordance with institutional and national guidelines and regulations for the care and use of laboratory animals.

References

1. Hartley JL, Davenport M, Kelly DA. Biliary atresia. Lancet 2009;374:1704-13.
2. Ortiz-Perez A, Donnelly B, Temple H, et al. Innate Immunity and Pathogenesis of Biliary Atresia. Front Immunol 2020;11:329.
3. Ye C, Zhu J, Wang J, et al. Single-cell and spatial transcriptomics reveal the fibrosis-related immune landscape of biliary atresia. Clin Transl Med 2022;12:e1070.
4. Zhang M, Serna-Salas S, Damba T, et al. Hepatic stellate cell senescence in liver fibrosis: Characteristics, mechanisms and perspectives. Mech Ageing Dev 2021;199:111572.
5. Kisseleva T, Brenner D. Molecular and cellular mechanisms of liver fibrosis and its regression. Nat Rev Gastroenterol Hepatol 2021;18:151-66.
6. Huarte M. The emerging role of lncRNAs in cancer. Nat Med 2015;21:1253-61.
7. Zhan DT, Xian HC. Exploring the regulatory role of lncRNA in cancer immunity. Front Oncol 2023;13:1191913.
8. Toden S, Zumwalt TJ, Goel A. Non-coding RNAs and potential therapeutic targeting in cancer. Biochim Biophys Acta Rev Cancer 2021;1875:188491.
9. Kim VN. MicroRNA biogenesis: coordinated cropping and dicing. Nat Rev Mol Cell Biol 2005;6:376-85.
10. Iwakawa HO, Tomari Y. The Functions of MicroRNAs: mRNA Decay and Translational Repression. Trends Cell Biol 2015;25:651-65.
11. Yang Y, Jin Z, Dong R, et al. MicroRNA-29b/142-5p contribute to the pathogenesis of biliary atresia by regulating the IFN-gamma gene. Cell Death Dis 2018;9:545.
12. Ogawa T, Enomoto M, Fujii H, et al. MicroRNA-221/222 upregulation indicates the activation of stellate cells and the progression of liver fibrosis. Gut 2012;61:1600-9.
13. Shen WJ, Dong R, Chen G, et al. microRNA-222 modulates liver fibrosis in a murine model of biliary atresia. Biochem Biophys Res Commun 2014;446:155-9.
14. Dong R, Zheng Y, Chen G, et al. miR-222 overexpression may contribute to liver fibrosis in biliary atresia by targeting PPP2R2A. J Pediatr Gastroenterol Nutr 2015;60:84-90.
15. Yu F, Zheng J, Mao Y, et al. Long Non-coding RNA Growth Arrest-specific Transcript 5 (GAS5) Inhibits Liver Fibrogenesis through a Mechanism of Competing Endogenous RNA. J Biol Chem 2015;290:28286-98.
16. Coutant A, Rescan C, Gilot D, et al. PI3K-FRAP/mTOR pathway is critical for hepatocyte proliferation whereas

MEK/ERK supports both proliferation and survival. Hepatology 2002;36:1079-88.
17. Yoshida T, Delafontaine P. Mechanisms of IGF-1-Mediated Regulation of Skeletal Muscle Hypertrophy and Atrophy. Cells 2020;9:1970.
18. Takahashi Y. The Role of Growth Hormone and Insulin-Like Growth Factor-I in the Liver. Int J Mol Sci 2017;18:1447.
19. Adamek A, Kasprzak A. Insulin-Like Growth Factor (IGF) System in Liver Diseases. Int J Mol Sci 2018;19:1308.
20. Mederacke I, Dapito DH, Affò S, et al. High-yield and high-purity isolation of hepatic stellate cells from normal and fibrotic mouse livers. Nat Protoc 2015;10:305-15.
21. Yang L, Shivakumar P, Kinder J, et al. Regulation of bile duct epithelial injury by hepatic CD71+ erythroid cells. JCI Insight 2020;5:e135751.
22. Mohanty SK, Donnelly B, Dupree P, et al. A Point Mutation in the Rhesus Rotavirus VP4 Protein Generated through a Rotavirus Reverse Genetics System Attenuates Biliary Atresia in the Murine Model. J Virol 2017;91:e00510-17.
23. Nio M, Ohi R, Miyano T, et al. Five- and 10-year survival rates after surgery for biliary atresia: a report from the Japanese Biliary Atresia Registry. J Pediatr Surg 2003;38:997-1000.
24. Petersen C, Harder D, Abola Z, et al. European biliary atresia registries: summary of a symposium. Eur J Pediatr Surg 2008;18:111-6.
25. Lee M, Chen SC, Yang HY, et al. Infant Stool Color Card Screening Helps Reduce the Hospitalization Rate and Mortality of Biliary Atresia: A 14-Year Nationwide Cohort Study in Taiwan. Medicine (Baltimore) 2016;95:e3166.
26. Khurana A, Sayed N, Allawadhi P, Weiskirchen R. It's all about the spaces between cells: role of extracellular matrix in liver fibrosis. Ann Transl Med 2021;9:728.
27. He W, Dai C. Key Fibrogenic Signaling. Curr Pathobiol Rep 2015;3:183-92.
28. Lang Z, Zhang R, Li X, et al. GAS5-inhibited hepatocyte pyroptosis contributes to hepatic stellate cell inactivation via microRNA-684 and AHR. iScience 2023;26:107326.
29. Smith CM, Steitz JA. Classification of gas5 as a multi-small-nucleolar-RNA (snoRNA) host gene and a member of the 5'-terminal oligopyrimidine gene family reveals common features of snoRNA host genes. Mol Cell Biol 1998;18:6897-909.
30. Mourtada-Maarabouni M, Pickard MR, Hedge VL, et al. GAS5, a non-protein-coding RNA, controls apoptosis and is downregulated in breast cancer. Oncogene 2009;28:195-208.
31. Sun M, Jin FY, Xia R, et al. Decreased expression of long noncoding RNA GAS5 indicates a poor prognosis and promotes cell proliferation in gastric cancer. BMC Cancer 2014;14:319.
32. Yacqub-Usman K, Pickard MR, Williams GT. Reciprocal regulation of GAS5 lncRNA levels and mTOR inhibitor action in prostate cancer cells. Prostate 2015;75:693-705.
33. Xiu AY, Ding Q, Li Z, et al. Doxazosin Attenuates Liver Fibrosis by Inhibiting Autophagy in Hepatic Stellate Cells via Activation of the PI3K/Akt/mTOR Signaling Pathway. Drug Des Devel Ther 2021;15:3643-59.
34. Ye Y, Li Z, Feng Q, et al. Downregulation of microRNA-145 may contribute to liver fibrosis in biliary atresia by targeting ADD3. PLoS One 2017;12:e0180896.
35. Kumar P, Raeman R, Chopyk DM, et al. Adiponectin inhibits hepatic stellate cell activation by targeting the PTEN/AKT pathway. Biochim Biophys Acta Mol Basis Dis 2018;1864:3537-45.
36. Bezerra JA. Potential etiologies of biliary atresia. Pediatr Transplant 2005;9:646-51.
37. Coots A, Donnelly B, Mohanty SK, et al. Rotavirus infection of human cholangiocytes parallels the murine model of biliary atresia. J Surg Res 2012;177:275-81.
38. Mohanty SK, Lobeck I, Donnelly B, et al. Rotavirus Reassortant-Induced Murine Model of Liver Fibrosis Parallels Human Biliary Atresia. Hepatology 2020;71:1316-30.

Cite this article as: Wang R, Gao Y. Long non-coding RNA growth arrest-specific 5 inhibits liver fibrogenesis in biliary atresia by interacting with microRNA-222 and repressing IGF1/AKT signaling. Transl Pediatr 2023;12(12):2107-2120. doi: 10.21037/tp-23-424